Short stack modeling of degradation in solid oxide fuel cells
Part II. Sensitivity and interaction analysis

J.I. Gazzarri [a], O. Kesler [b],*

[a] Department of Mechanical Engineering, University of British Columbia, 2054-6250 Applied Science Lane, Vancouver, BC V6T 1Z4, Canada
[b] Department of Mechanical and Industrial Engineering, University of Toronto, 5 King's College Road, Toronto, ON M5S 3G8, Canada

Abstract

In the first part of this two-paper series, we presented a numerical model of the impedance behaviour of a solid oxide fuel cell (SOFC) aimed at simulating the change in the impedance spectrum induced by contact degradation at the interconnect-electrode, and at the electrode–electrolyte interfaces. The purpose of that investigation was to develop a non-invasive diagnostic technique to identify degradation modes in situ. In the present paper, we appraise the predictive capabilities of the proposed method in terms of its robustness to uncertainties in the input parameters, many of which are very difficult to measure independently. We applied this technique to the degradation modes simulated in Part I, in addition to anode sulfur poisoning. Electrode delamination showed the highest robustness to input parameter variations, followed by interconnect oxidation and interconnect detachment. The most sensitive degradation mode was sulfur poisoning, due to strong parameter interactions. In addition, we simulate several simultaneous two-degradation-mode scenarios, assessing the method's capabilities and limitations for the prediction of electrochemical behaviour of SOFC's undergoing multiple simultaneous degradation modes.
© 2007 Elsevier B.V. All rights reserved.

Keywords: SOFC; Degradation; Diagnosis; Sensitivity analysis; Impedance spectroscopy; Delamination

1. Introduction

In the first part of this series, we presented a numerical model of the ac behaviour of an SOFC to explore the possibility to diagnose degradation using impedance spectroscopy in a minimally invasive way. Simulated degradation mechanisms included electrode delamination, interconnect oxidation, and interconnect detachment [1,2]. In a separate work, we had previously presented results for microstructural degradation modes such as sulfur poisoning [3]. The distinct impact of these degradation modes on the impedance spectrum suggested ways to identify them. Examples of distinct patterns induced by degradation are the behaviour of the series and polarization resistance with progressing extent of degradation, and the change in electrode arc size and/or characteristic frequency. According to our modeling results, electrode delamination causes a simultaneous and equivalent increase in both series and polarization resistance,

in proportion to the amount of delaminated area. At the same time, the electrode characteristic frequencies remain unchanged because delamination does not alter the electrochemical nature of the cell reactions. Interconnect oxidation, on the other hand, degrades cell performance by increasing the series resistance, without much change in either polarization resistance or relaxation frequencies [1]. Interconnect detachment, a third type of contact degradation, mainly affects series resistance with some polarization resistance deterioration, especially for large detached areas [1]. Finally, sulfur poisoning deteriorates cell performance by mainly affecting polarization resistance, without change in series resistance, at least at early stages when the effect is still reversible. As with any numerical model, it is of utmost importance utilize reliable input parameters in order to achieve sensible results. In this work, a multivariable interaction study revealed how the model results vary with different combinations of input parameters. This study aims at providing insight on the impact of inaccurate input data on the modeling results. In such a complex model as that of an operating SOFC, many of the model input parameters are very difficult to determine experimentally by independent measurements, leading to

---

the use of estimates of unclear accuracy, or to considering of some of the parameters as fitting parameters. In this work we present a multivariable sensitivity analysis study based on the uniform design experimental design method [4] that evaluates the influence of varying each of the input parameters over a wide yet reasonable range.

A parametric study consisting of calculating the polarization and series resistances for a wide range of input parameters revealed some of the strengths and limitations of the method. Repeated for all degradation modes presented in [1] plus sulfur poisoning, this parameterization revealed that the results for delamination are very robust to inaccuracies in, or interactions among, cell parameters. A similar conclusion applies to oxide layer growth and interconnect detachment, but to a lesser extent. In contrast, the results for sulfur poisoning are strongly dependent on the operating conditions and cell characteristics, especially the operating voltage and the charge transfer coefficients.

The modeling results presented in Part I [1] and in [3] show the impact of individual degradation modes on the impedance spectrum, suggesting ways to diagnose them based on the identification of the induced changes. A situation not previously considered, however, is the simultaneous occurrence of multiple degradation modes. Natural questions arising from this idea are:

1. Is it possible to diagnose multiple degradation mechanisms occurring simultaneously?
2. Are their effects additive? Could different degradation modes interact in such a way as to obscure the effect of one or more of them?

This work explores possible scenarios of simultaneous degradation modes, assessing the capabilities and limitations of the proposed method. A convenient method to visualize the effect of multiple simultaneous degradation modes is presented that allows a better interpretation of the trend in resistances.

2. Results and discussion

2.1. Sensitivity and parameter interaction analysis

Using realistic input parameters is of utmost importance in any numerical model. This is especially true in very complex models such as that of a fuel cell, because many important parameters are not independently or readily measurable. Charge transfer coefficients, electroactive surface area, exchange current density, and tortuosity are typical examples. Moreover, different combinations of parameters may yield the same modeling results, making the model prone to ambiguities, and making unambiguous model validation extremely difficult. Defining parameters as fitting, or free, parameters is common practice in the modeling literature, but it must be done with care, since it is easy to obtain apparently sensible results, using unrealistic input data. This difficult problem, inherent to every numerical model, suggests the need for a method to assess the sensitivity of the results to inaccuracies in the input data. One objective of this work is to utilize a statistical method to determine the

impact of those inaccuracies on the model output. This method is based on the uniform design technique [4], which consists of designing a set of experiments using different combinations of input variables to evaluate their relative influence on the results and their potential interactions. In the present case, we run a certain study case several times using a broad, yet reasonable, range of variability for each input parameter, and compare the results. If the obtained scatter is of the order of the expected experimental scatter, then it can be concluded that the simulation is reasonably insensitive to inaccuracies in the input data. On the other hand, if the dispersion is significant, the critical input parameters that are most responsible for the scatter should be identified and, if possible, their values should be estimated with higher accuracy. This study is of especial importance in a complicated system such as a fuel cell, since its many concurrent physical mechanisms may interact with each other, yielding unexpected results if not properly taken into account.

The cross influence between electrodes is an example of this kind of interaction. The polarization resistance of an electrode is inversely proportional to the total current density in the Tafel regime, as long as the system is not under mass transport control. If one electrode loses electrochemical activity due to microstructural degradation, the overall cell polarization state will change. This will change, in particular, the polarization state of the other electrode if the cell is working in potentiostatic mode, thereby changing its polarization resistance. Therefore, both electrode polarization resistances will change due to a performance loss of just one electrode.

The Uniform Design method specifies a combination of factors to be used for a given number of runs of the desired experiment. The factors correspond to the input parameters whose effect on the result we want to characterize, 20 in the present case, as specified in Table 1. The number of runs chosen in this case is thirty. The next sections present the normalized resistance results for a certain extent of degradation for each individual degradation mode, calculated 30 times using the parameter grid specified in Table 1. The dispersion in the normalized resistance results indicates the robustness of the method for each degradation mode to input parameter variability. For each case in which the dispersion is considerable, we explore its possible causes and suggest strategies for improvement. Table 2 details the parameter combinations used for the case of delamination: 21 factors in 30 runs.

2.1.1. Delamination

In the case of electrode delamination, a distinct trend followed by both the normalized series and polarization resistances as a function of progressively increasing electrode delaminated area appeared as a suitable means to identify this type of degradation mode [1,2]. For example, for a 36% loss in delaminated area, both normalized resistance values become:

$$\bar{R}_S = \frac{R_S^0}{R_S} \approx 0.64 \qquad \bar{R}_P = \frac{R_P^0}{R_P} \approx 0.64,$$

where the superscript zero indicates the resistance prior to degradation.

Table 1
Range of variability of input parameters for the sensitivity analysis of the results

Parameter	Symbol	Min	Max	Units
Anode (ESC) and cathode thickness (ESC, ASC)	t_{ANO}, t_{CAT}	10	100	μm
Anode (ASC) thickness	t_{ANO}	500	1000	μm
Electrolyte thickness (ESC)	t_{ELY}	90	200	μm
Electrolyte thickness (ASC)	t_{ELY}	5	20	μm
Channel hydrogen partial pressure	pH_2	0.1	0.97	atm
Channel oxygen partial pressure	pO_2	0.1	0.21	atm
Operating point as a fraction of the OCV	V_{CELL}	0.2	0.99	–
Anode charge transfer coefficient, anodic direction	α_{AA}	0.5	2	–
Anode charge transfer coefficient, cathodic direction	α_{AC}	0.2	1	–
Cathode charge transfer coefficient, anodic direction	α_{CA}	0.5	2	–
Cathode charge transfer coefficient, cathodic direction	α_{CC}	0.2	1	–
Anode and cathode active surface area	S_{ano}, S_{cat}	10^5	10^6	m^{-1}
Anode and cathode porosity	ε	0.1	0.7	–
Anode and cathode gas phase tortuosity	τ	2	7	–
Log anode double layer capacitance	$C_{dl, ano}$	−1	2	$F\,m^{-2}$
Log cathode double layer capacitance	$C_{dl, cat}$	−1	2	$F\,m^{-2}$
Log anode exchange current density	$i_{0, ANO}$	1	3	$A\,m^{-2}$
Log cathode exchange current density	$i_{0, CAT}$	1	3	$A\,m^{-2}$
Delamination thickness (if applicable)	t	0.1	5	μm

In order to assess the sensitivity of these results to input parameter inaccuracies and indetermination, as well as to possible unexpected parameter interaction, 21 parameters were varied over the range shown in Table 1, using a 30-run set of numerical experiments. Each parameter takes 30 different values, equally spaced over an interval that spans a broad, yet reasonable, range of variability, for a fixed extent of degradation. Each run consists of the solution of the system of equations to calculate the normalized resistances for a different combination of parameters, chosen according to the uniform design criterion.

Fig. 1 shows the geometry used for the simulations. Fig. 2 shows the results for both normalized series and polarization
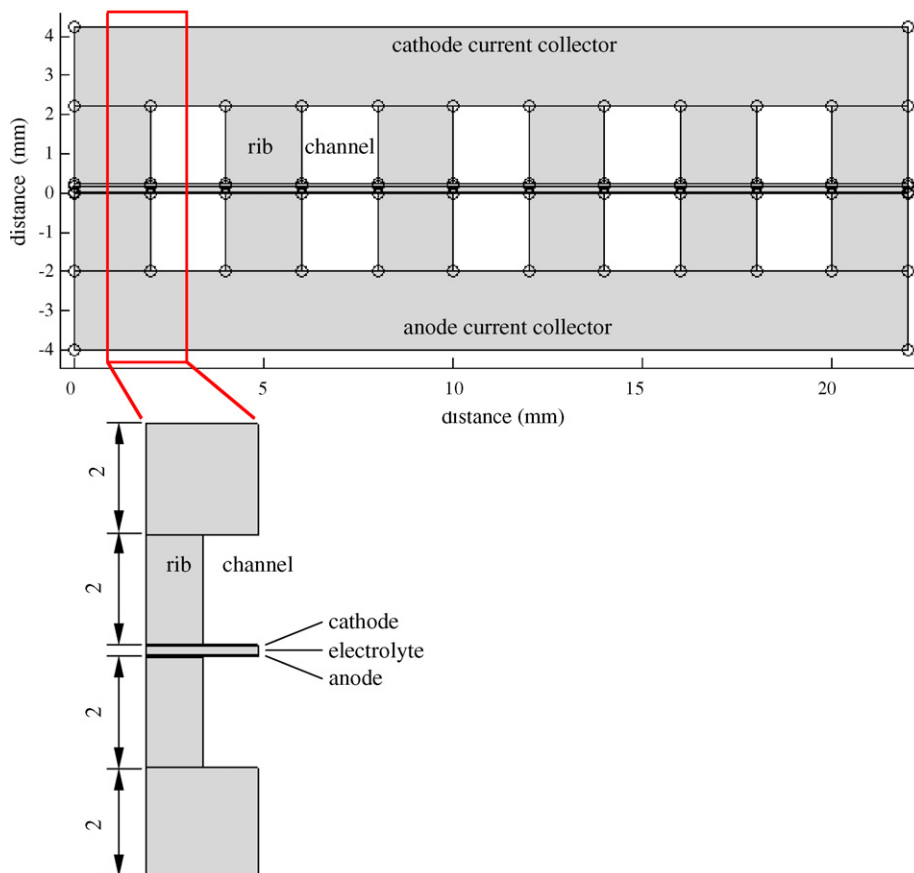

Fig. 1. The cell geometry used for the sensitivity and parameter interaction studies.

Table 2
Parameter variation for the uniform design analysis corresponding to delamination

t_{ANO}	t_{CAT}	t_{ELY}	pH_2	pO_2	V	α_{AA}	α_{AC}	α_{CA}	α_{CC}	S_{ano}	S_{cat}	ε_{ano}	ε_{cat}	τ_{ano}	τ_{cat}	$C_{dl, ano}$	$C_{dl, cat}$	$i_{0, ANO}$	$i_{0, CAT}$	t
3.17E−05	9.38E−05	1.51E−04	0.19	0.10	0.39	0.9	0.3	1.3	0.8	4.72E+05	8.76E+05	0.33	0.16	4.4	3.9	24.0	0.4	16	42	7.76E−07
5.03E−05	3.79E−05	1.09E−04	0.73	0.10	0.88	1.8	0.7	0.5	0.7	4.41E+05	5.03E+05	0.66	0.56	6.5	6.7	4.5	2.8	36	12	1.28E−06
3.48E−05	7.21E−05	1.28E−04	0.46	0.14	0.55	1.7	0.7	1.4	0.6	1.00E+05	3.79E+05	0.37	0.70	2.2	3.0	0.1	0.1	92	1000	2.69E−07
2.86E−05	1.62E−05	1.54E−04	0.91	0.11	0.66	1.1	0.5	1.5	0.5	6.90E+05	1.62E+05	0.14	0.45	6.1	5.4	62.1	0.2	108	728	3.82E−06
5.34E−05	5.03E−05	1.96E−04	0.25	0.15	0.45	0.7	0.4	0.6	0.7	8.14E+05	4.41E+05	0.64	0.35	6.7	2.3	0.2	0.5	386	281	3.31E−06
6.59E−05	5.97E−05	1.20E−04	0.20	0.20	0.20	0.6	0.6	0.9	0.2	4.10E+05	2.24E+05	0.43	0.37	3.2	6.3	7.3	0.1	30	30	4.16E−06
1.62E−05	8.14E−05	1.24E−04	0.88	0.18	0.77	1.4	0.9	0.8	0.9	5.97E+05	9.07E+05	0.45	0.20	5.1	6.1	0.2	0.2	204	240	2.30E−06
9.07E−05	2.55E−05	1.36E−04	0.61	0.12	0.74	1.0	0.3	0.8	0.8	1.93E+05	4.10E+05	0.22	0.14	3.4	4.9	0.1	24.0	67	36	3.48E−06
7.83E−05	2.86E−05	1.01E−04	0.82	0.13	0.28	1.4	0.4	1.1	0.3	3.79E+05	2.55E+05	0.49	0.18	5.3	3.2	11.7	5.7	853	204	6.07E−07
4.10E−05	5.34E−05	9.76E−05	0.13	0.17	0.80	1.5	0.3	1.1	1.0	9.38E+05	1.00E+05	0.16	0.49	2.5	3.4	2.2	1.7	12	127	2.13E−06
4.72E−05	4.10E−05	1.89E−04	0.70	0.17	0.34	0.8	0.8	1.8	0.8	2.24E+05	5.34E+05	0.18	0.27	2.9	6.8	5.7	0.9	530	386	1.45E−06
8.76E−05	8.45E−05	1.58E−04	0.94	0.20	0.42	1.8	0.4	1.6	0.7	5.03E+05	2.86E+05	0.12	0.47	4.2	2.7	0.3	3.6	329	10	1.96E−06
5.66E−05	4.72E−05	9.00E−05	0.49	0.18	0.61	0.5	0.5	1.9	0.9	1.31E+05	9.38E+05	0.41	0.58	7.0	3.7	78.8	78.8	281	92	2.47E−06
8.45E−05	4.41E−05	1.92E−04	0.79	0.16	0.72	1.3	0.9	1.0	0.4	2.86E+05	8.14E+05	0.29	0.64	4.9	2.5	18.9	0.3	14	16	3.14E−06
7.52E−05	6.90E−05	2.00E−04	0.52	0.16	0.99	2.0	0.4	1.9	0.6	7.83E+05	3.48E+05	0.39	0.22	4.6	6.5	14.9	100.0	19	853	2.80E−06
6.90E−05	0.0001	9.38E−05	0.64	0.13	0.31	1.6	0.9	2.0	0.3	9.69E+05	5.66E+05	0.24	0.29	6.8	4.4	1.1	0.7	49	67	2.97E−06
1.93E−05	9.07E−05	1.70E−04	0.67	0.18	0.36	1.6	0.2	0.7	0.4	3.17E+05	6.28E+05	0.60	0.53	3.6	4.6	48.9	14.9	57	329	3.65E−06
8.14E−05	1.31E−05	1.32E−04	0.34	0.19	0.91	1.2	0.2	1.8	0.3	7.21E+05	6.59E+05	0.62	0.62	4.1	5.1	0.3	0.3	174	108	1.11E−06
3.79E−05	7.52E−05	1.05E−04	0.76	0.15	0.53	0.9	0.3	1.3	0.4	8.45E+05	7.83E+05	0.27	0.66	4.8	7.0	0.9	30.4	621	19	4.32E−06
2.24E−05	2.24E−05	1.77E−04	0.55	0.19	0.23	1.1	0.9	1.0	0.8	8.76E+05	3.17E+05	0.35	0.60	5.4	4.8	0.7	48.9	26	79	4.38E−07
5.97E−05	1.00E−05	1.47E−04	0.16	0.14	0.50	1.9	1.0	0.6	0.3	5.34E+05	8.45E+05	0.10	0.43	2.0	5.8	3.6	62.1	240	174	2.63E−06
6.28E−05	3.48E−05	1.39E−04	0.97	0.21	0.58	1.0	0.7	1.4	0.6	9.07E+05	1.00E+06	0.70	0.12	3.0	3.6	2.8	4.5	10	452	5.00E−06
2.55E−05	1.93E−05	1.13E−04	0.37	0.15	0.47	1.7	0.8	1.7	0.9	7.52E+05	4.72E+05	0.56	0.24	3.9	2.0	38.6	9.2	149	14	3.99E−06
1.31E−05	5.66E−05	1.85E−04	0.85	0.11	0.83	0.6	0.6	1.7	0.2	6.28E+05	6.90E+05	0.47	0.39	2.3	2.2	0.5	18.9	42	57	1.62E−06
9.69E−05	6.28E−05	1.43E−04	0.22	0.12	0.25	1.3	0.6	1.6	1.0	3.48E+05	7.52E+05	0.51	0.51	5.6	6.0	0.4	7.3	22	530	4.49E−06
9.38E−05	7.83E−05	1.17E−04	0.31	0.19	0.85	0.8	0.8	0.7	0.5	6.59E+05	5.97E+05	0.20	0.33	5.8	2.9	30.4	11.7	79	621	9.45E−07
1.00E−05	3.17E−05	1.66E−04	0.28	0.21	0.96	1.9	0.6	1.2	0.5	1.62E+05	7.21E+05	0.31	0.31	6.0	4.2	1.4	1.4	1000	49	4.83E−06
7.21E−05	9.69E−05	1.62E−04	0.58	0.12	0.94	0.7	1.0	1.2	0.9	5.66E+05	1.93E+05	0.58	0.68	3.7	4.1	9.2	2.2	728	149	4.66E−06
4.41E−05	8.76E−05	1.73E−04	0.10	0.16	0.69	1.2	0.8	1.5	0.4	2.55E+05	1.31E+05	0.68	0.10	6.3	5.3	1.7	38.6	127	22	1.79E−06
0.0001	6.59E−05	1.81E−04	0.43	0.13	0.64	1.5	0.5	0.9	0.6	1.00E+06	9.69E+05	0.53	0.41	2.7	5.6	100.0	1.1	452	26	1.00E−07

The order given in Table 1 is preserved for the varied parameters, which are listed across the columns. Each row corresponds to one numerical experiment, using the values in that row for each parameter that is varied. SI units are used throughout the table.
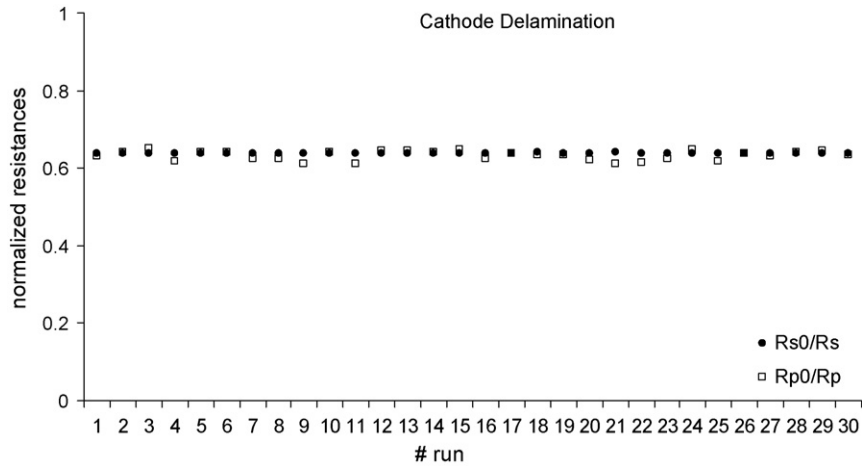
Fig. 2. Normalized resistance results for a delamination equivalent to 36% of the cathode length (two ribs and two channel lengths) are almost insensitive to input parameter variation, and no unexpected interaction is apparent.
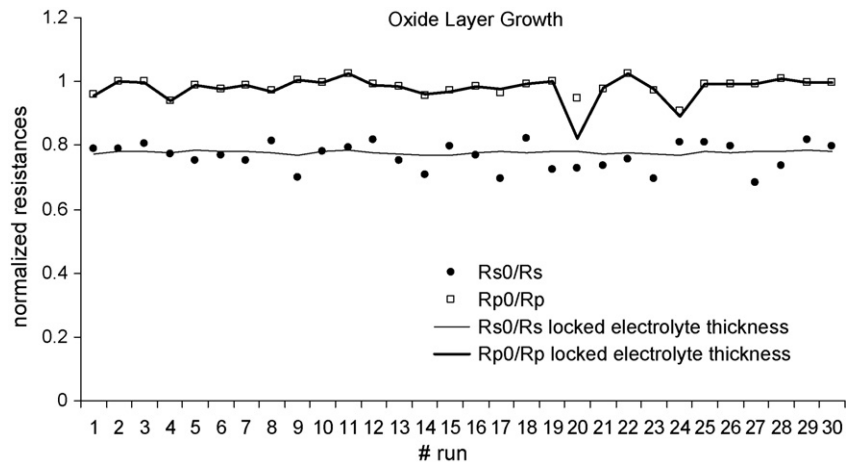

Fig. 3. Some variability is observed in the normalized resistance results for growth of a 5 μm oxide layer on the interconnect. The variability in polarization resistance (empty squares) is associated with the non-monotonic dependence of the cathode polarization resistance on overall polarization (see text). The presence of the electrolyte thickness among the varied factors causes variability in normalized series resistance (solid circles vs. thin line).

resistances. It is apparent from the graph that their sensitivity to variations in the input parameters is very small. This result shows that the model predictions of normalized resistance behaviour caused by delamination are robust to variability in the input parameters. This invariance is associated with the nature of delamination itself. Electrode delamination deteriorates the cell performance by interrupting the flow of ionic charge, thereby deactivating the cell volumes above and below the delamination because of the large aspect ratio of the cell. This phenomenon is of a conductance nature, and it will have an equivalent effect for all reasonable cell geometries and electrochemical characteristics. The normalized series resistance for run k can be approximated as[1]:

$$\frac{R_S^0(k)}{R_S(k)} = \frac{R_S^0(k)}{R_S^0(k)(A^0/(A^0 - A^D))} = 1 - \frac{A^D}{A^0} \tag{1}$$

---

[1] This approximation implies neglecting any in-plane conduction.

where A^0 and A^D are the intact projected area and the delaminated area, respectively. Eq. (1) shows that the normalized series resistance is independent of the intact series resistance. This property makes the series resistance behaviour in the case of electrode delamination different from that corresponding to the following case studied: oxide layer growth.

2.1.2. Oxide layer growth

If the same concept is applied to oxide layer growth on the interconnect, the variability is larger, as shown in Fig. 3, which illustrates the scatter in normalized series and polarization resistances for a 5 μm thick oxide layer simulated between the cathode and its corresponding interconnect. The variability in normalized series resistance is a result of the impact of the oxide layer on the cell impedance. Unlike the case of delamination, the normalized series resistance does depend on the value of the intact series resistance. An oxide layer of fixed thickness increases the series resistance by a constant value in all runs:
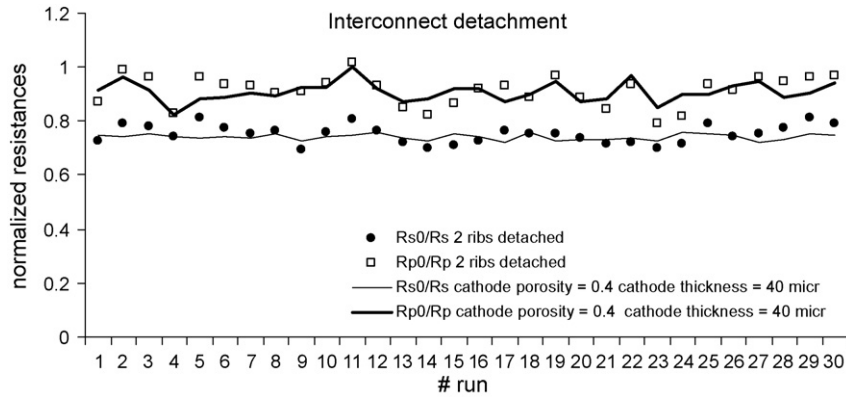
Fig. 4. Both series and polarization resistance show a variability that is comparable to that of oxide layer growth. Cathode porosity and thickness, the factors that affect cathode conductance the most, are responsible for the series resistance variability (solid circles). When these parameters are locked at the default values, the series resistance variability decreases (thin line).

$$\frac{R_S^0(k)}{R_S(k)} = \frac{R_S^0(k)}{R_S^0(k) + \delta} \tag{2}$$

where δ is a constant that depends on the oxide layer thickness and conductivity. The intact series resistance is different in all cases, since the electrolyte thickness, by far the most important contributor, is among the varied parameters. Therefore, the scatter in the normalized series resistance is a result of the scatter in the intact series resistance. When the numerical experiment is repeated excluding the electrolyte thickness variability, the series resistance scatter disappears, as shown in Fig. 3 (thin line). The dispersion in polarization resistance is the result of an interaction between the increase in series resistance due to the oxide layer and the polarization resistance, via the polarization resistance dependence on the total current density. The polarization resistance of an electrode depends, among other factors, on current density. An increase in total resistance lowers the delivered current when the cell is operated in potentiostatic mode, hence changing the polarization resistance of the electrodes. Section 2.1.4 addresses this phenomenon in further detail.

2.1.3. Interconnect detachment

The variability in the case of interconnect detachment is comparable to that of oxide layer growth, as shown in Fig. 4. The

reason for the series resistance scatter, however, is not the same one described in Section 2.1.2. The electronic conductivity of the cathode largely influences the resulting series resistance after cathode-interconnect interface detachment, because of an effective increase in the electronic path length. The increase in series resistance becomes, therefore, dependent on the two factors that determine the electronic conductance for a given material: cathode porosity and cathode thickness. Upon detachment, the series resistance will increase to a greater extent for high cathode porosity and low cathode thickness. When cathode thickness and cathode porosity remain fixed at the default values, the dispersion in series resistance diminishes considerably, as shown by the thin line in Fig. 4.

The scatter in polarization resistance is related to the different amount of shadowing produced by the detachment among runs. Shadowing is the partial deactivation of projected cell area caused by a degradation mechanism affecting contact resistance at an interface, and it manifests itself as an increase in polarization resistance. An interfacial problem at the interconnect-cathode boundary causes an extent of shadowing that depends on the cathode electronic resistance in the in-plane direction, since incoming electrons must circumvent the affected interconnect ribs in order to reach the cathode. For large amounts of detachment, the relative effect of relevant cathode parameters
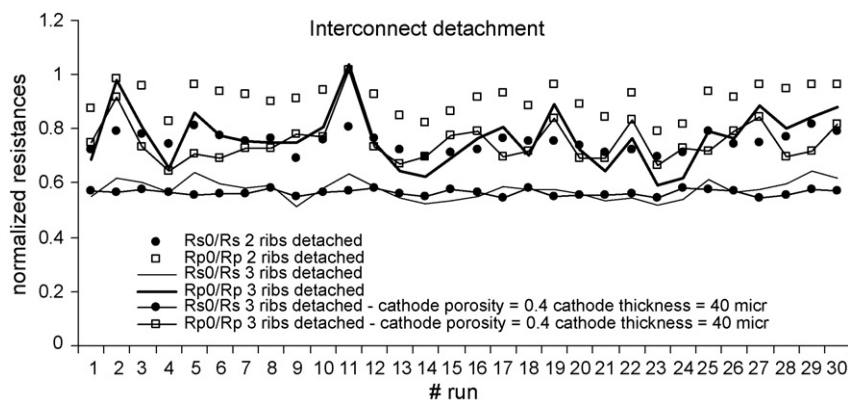

Fig. 5. Both R_p magnitude and R_p scatter increase when the number of detached ribs increases from 2 to 3. Equivalently to the two-rib detachment case, the scatter in R_s decreases upon locking the parameters relevant to cathode electronic conductance: cathode porosity and thickness.
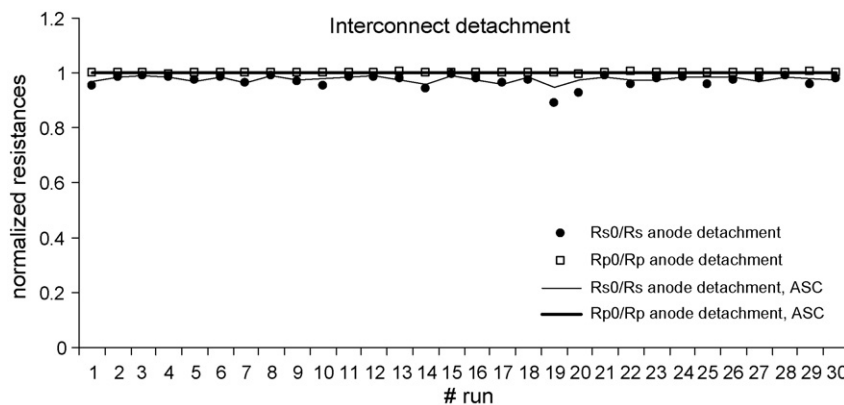
Fig. 6. Interconnect detachment on the anode side presents a lower scatter, because of the very high electronic conductance of the anode.

on in-plane resistance is large; hence the larger scatter in the resulting polarization resistance. Fig. 5 clearly shows this trend, comparing the effect of two- and three-rib detachments on the normalized resistances.

Fig. 6 shows that there is a relatively small scatter in the case of interconnect detachment on the anode side, providing further evidence of the influence of electronic conductance on the variability in the results. The very high conductance provided by metallic nickel accommodates the electronic current redistribution relatively easily, largely regardless of the input parameter combination. This statement is especially true for anode-supported cells, because of their very thick anode layer.

2.1.4. Sulfur poisoning

There is experimental evidence of the fact that sulfur poisoning deteriorates SOFC anodes by adsorbing on electroactive reaction sites as a monolayer [5], particularly at early stages in the poisoning process. If this assumption holds, sulfur poisoning is expected to affect the electrochemistry by a direct decrease in surface area, without severe influence on microstructure morphology (porosity and tortuosity), and hence on the mass transport characteristics of the porous electrode. In [5], the authors also provide evidence of invariance in charge transfer coefficients, by showing single electrode polarization curves

before and after poisoning. Based on these observations, our approach has been to simulate sulfur poisoning by decreasing the electroactive surface area (S_{ANO} in Eq. (4) in [1]). Furthermore, these characteristics make sulfur poisoning different from carbon deposition, another microstructural degradation mode affecting the anode due to hydrocarbon cracking. In this case, solid deposits of carbon on the surface of the material may partially block the pores in the anode, and thereby also affect the diffusional characteristics of the anode microstructure. It therefore is not possible to simulate it with the model in its present form without additional experimental information regarding the extent of pore blockage for a given extent of carbon deposition and its corresponding surface area loss. More information is needed on how the relevant microstructural parameters are affected by the presence of solid carbon in the Ni–YSZ matrix.

Prediction of the electrochemical signatures associated with this degradation mode is the most severely influenced by input parameter variability, because the effects are electrochemical in nature. The large variability in R_p shown in Fig. 7, empty squares, illustrates this statement. As explained in the introduction, the high complexity of the SOFC electrochemistry causes component interdependencies that may mislead an attempt to diagnose a single degradation event. The reason for this variability is the current density dependence of the polarization
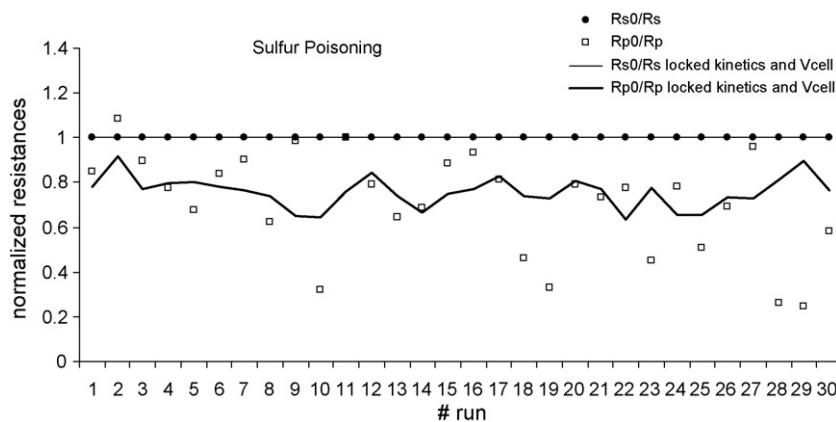

Fig. 7. Sulfur poisoning inducing 90% loss in the active anode area. While the normalized series resistance shows no variability (solid circles and thin line), a high level of interaction among parameters yields a large variability in the results for polarization resistance (empty squares). The variability is much smaller when kinetic parameters, inlet partial pressures, and operating point are fixed (thick line). These calculations were done using the half-rib, half-channel geometry shown in Fig. 1.

resistance, and the fact that the simulation is set as potentiostatic. The Butler–Volmer kinetics assumed dominant at the electrodes implies a non-monotonic behaviour of the polarization resistance with polarization state for cathodes with different charge transfer coefficients in each reaction direction. At constant dc potential, the reduction in anode electrochemical activity due to poisoning decreases the current density of the cell, and this change modifies the polarization resistance of *both* electrodes. The polarization resistance of the cathode, according to this model, results from the reciprocal of the derivative of the Butler–Volmer source equation (Eq. (5), Part I [1]), with respect to the overpotential:

$$\frac{\partial i_{F,ION,CAT}(\eta)}{\partial \eta} = R_P^{-1} = \left[S_{CAT} i_{0,CAT} \left[f_{ca} \exp(f_{ca}\eta) + \left(\frac{c_{O_2}}{c_{O_2}^0} f_{cc} - \frac{1}{c_{O_2}^0} \frac{\partial c_{O_2}}{\partial \eta} \right) \exp(-f_{cc}\eta) \right] \right]^{-1}$$

Due to the different charge transfer coefficients in the anodic and cathodic directions, the cathode polarization resistance first increases, and then decreases for increasing overpotentials. Fig. 8 shows the cathode polarization resistance, calculated parametrically as a function of applied overpotential, for this model. This figure shows three operating points: (A) the intact case; (B) the state after some mild change in total current density; (C) a severely degraded case. These two degraded states can occur due to different extents of sulfur poisoning that change the overall delivered current density, and therefore, the polarization state of the cathode, even when degradation occurred at the anode. B and C indicate an increase and a decrease in polarization resistance, respectively, compared to the intact state A. The non-monotonic behaviour of R_p with cathodic overpotential is responsible for this behaviour. There is *interaction* between the amount of sulfur poisoning and the operating point. Consequently, to diagnose sulfur poisoning it is essential to have access to information such as the degradation history, since the initial and final state of resis-

tances may result in ambiguities. Fig. 7 shows, with a thick line, the normalized polarization resistance resulting from locking the operating voltage, exchange current densities, inlet partial pressures, and main charge transfer coefficients, α_{aa} and α_{cc}. The variability is clearly smaller, further confirming the analysis of the previous paragraph. Locking the other two charge transfer coefficients did not have an appreciable influence on the normalized resistance scatter, presumably because of their relatively low importance at the operating point considered in these runs. Table 3 summarizes the sensitivity analysis results for all the degradation modes under consideration.

2.2. The simultaneous occurrence of multiple degradation modes

Cathode delamination produces a simultaneous increase in series and polarization resistance. Sulfur poisoning, on the other hand, causes an increase in polarization resistance with little [5] or no [6,7] change in series resistance, since the conductive path for charge carriers remains essentially unaltered. Interconnect oxidation results almost exclusively in an increase in series resistance, while cathode-side interconnect detachment results in increased series resistance with some increase in polarization resistance. A conceivable degradation scenario could be the simultaneous occurrence of sulfur poisoning and interconnect oxidation such that both resulting normalized resistance ratios are approximately equal, as in the case of delamination. Based only on the initial and final states of series and polarization resistances, the two situations are indistinguishable. However, extra information may help in the diagnosis of such a combination of degradation modes:

1. Tracking the evolution of a single electrode arc or peak, in the case where this feature is reasonably deconvoluted from the other electrode features.
2. Tracking the cell degradation path to find a distinct pattern, based on previous knowledge about specific degradation mode kinetics.

For an explanation of each case, Table 4 details different stages of degradation in a simulated combined degradation scenario of interconnect oxide layer growth + sulfur poisoning, and independently, cathode delamination, producing approximately the same final values for normalized resistances. The characteristics of the combined degradation mode were estimated as follows: the anode active area decreases according to the equilibrium sulfur coverage at the operating temperature of 850 °C [8] for a fuel stream containing 10 ppm H$_2$S. This change causes a polarization resistance increase that is then matched to the series resistance increase caused, independently, by interconnect oxidation. A 4.3 μm thick oxide layer satisfies this requirement using the oxidation kinetics and chromia resistivity at the oper-
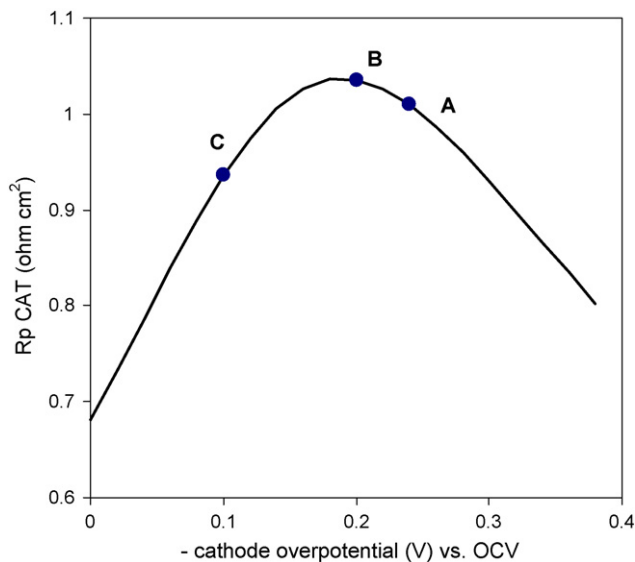

Fig. 8. Cathode polarization resistance dependence on overall (external) cathodic overpotential vs. 1.12 V. The overpotential at which the resistance is a maximum is a function of both cathode charge transfer coefficients.

Table 3

Average and percent deviation in normalized series and polarization resistance for the 30 uniform design runs, for each degradation mode, varying 20 (or 21, in the case of delamination) factors according to Table 1 Cases 1 and 2 indicate before and after locking the parameter identified as primary source of deviation

degradation type	config	interface or electrode affected	extent of degradation	Rs^0/Rs		Rp^0/Rp		parameter(s) responsible for dispersion
				mean	% stdev	mean	% stdev	
delamination	ESC	cathode / electrolyte	36% length	0.64	0.15	0.63	1.92	-
IC oxidation 1	ESC	cathode / interconnect	5 micron	0.77	5.44	0.98	2.55	t_{ELY}
IC oxidation 2	ESC	cathode / interconnect	5 micron	0.78	0.61	0.98	3.98	
IC detachment 1	ESC	cathode / interconnect	2 ribs	0.75	4.62	0.91	6.12	$\varepsilon_{CAT}, t_{CAT}$
IC detachment 2	ESC	cathode / interconnect	2 ribs	0.74	1.56	0.91	4.06	
IC detachment 1	ESC	cathode / interconnect	3 ribs	0.58	6.27	0.77	13.58	$\varepsilon_{CAT}, t_{CAT}$
IC detachment 2	ESC	cathode / interconnect	3 ribs	0.56	2.07	0.75	10.53	
IC detachment	ESC	anode / interconnect	2 ribs	0.97	2.29	1.00	0.17	-
IC detachment	ASC	anode / interconnect	2 ribs	0.98	1.08	1.00	0.02	-
sulfur poisoning 1	ESC	anode	90%	1.00	0.02	0.71	32.14	$\alpha_{AA} \, \alpha_{CC} \, V_{CELL}$ $i_{0,CAT} \, i_{0,ANO}$
sulfur poisoning 2	ESC	anode	90%	1.00	0.02	0.76	9.23	$p_{Hin} \, p_{Oin}$

Gray cells indicate relevant dispersion values affected by this change.

ating temperature [9,10] described in Chapter Four in [11]. Using this information, a combined degradation history is simulated, as shown in Table 4.

2.2.1. Tracking an individual electrode process

As explained in [3,11], the arc corresponding to the main anode process increases in diameter when the anode surface area decreases due to sulfur poisoning. Depending on the difference in relaxation frequencies between electrode processes, individual impedance arcs may be identifiable, in which case individual degradation mode diagnosis becomes easier. Fig. 9 illustrates this case for the first three stages in the simultaneous sulfur poisoning and oxide layer growth scenario of Table 4. The increase in R_p is solely due to the anode polarization resistance, unlike the case of delamination, where both electrode arcs increase, regardless of which one delaminates. In this case, the anode arc is clearly identifiable among the other features of the spectrum. In the case where it is not, Schichlein et al.'s [12] interesting method could be of aid, but care must be taken with the choice of data filtering and windowing strategy.

2.2.2. Tracking the degradation path

Different combinations of degradation modes may lead to the same final normalized resistances values. However, the differ-

ent degradation rates make unlikely that the degradation path followed by the system is equivalent in different cases. The concept of degradation space is introduced to clarify this point. The graph in Fig. 10 shows normalized polarization resistance versus normalized series resistance, with the extent of degradation as an implicit parameter. In this degradation space graph, point (1, 1) corresponds to the intact case.

Plotting the evolution of normalized series and polarization resistance starting at (1, 1) provides useful visual information about the nature and extent of degradation. A degradation mode that mainly affects R_s, like oxide layer growth, appears as an almost horizontal line progressing leftward with increasing extent of degradation. Sulfur poisoning, on the other hand, is reflected as a vertical line down from (1, 1), since it mainly affects the anodic R_p. Finally, a line at 45° from (1, 1) towards the origin represents delamination, because it causes a shadowing of the entire cell.

In this way, a combination of two or more modes will be, in general, a curve starting at (1, 1) and progressing downward and leftward, depending on the relative effect on series and polarization resistances. Regardless of its end point, the likelihood that two combinations will follow the same entire path is small and can reasonably be neglected, since each degradation mode has its own kinetics, with very different time scales at which

Table 4

Extent of degradation used in the example of combined degradation modes

Time (h)	Oxide layer growth oxide layer thickness (μm)	Sulfur poisoning fraction of active area loss
0	0.00	0
50	0.71	0.88[a]
508	2.25	0.88
967	3.11	0.88
1425	3.78	0.88
1884	4.34	0.88

[a] The large difference in kinetics of the two processes suggests that not considering the 2 h incubation period observed by Xia and Birss [5] is expected to be of no appreciable influence in this example.
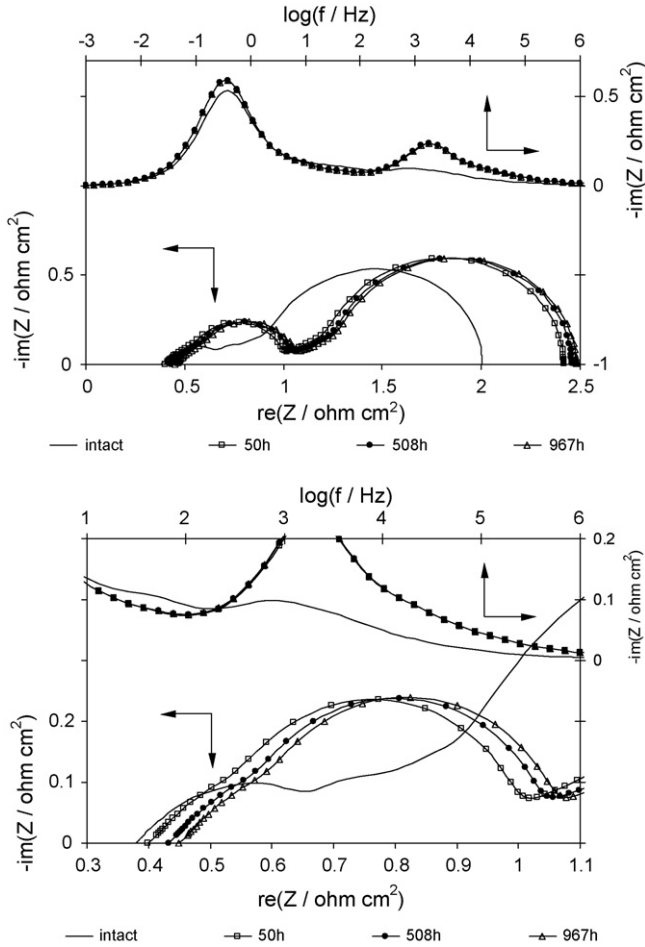
Fig. 9. Impedance spectra corresponding to three stages of combined sulfur poisoning + interconnect oxidation degradation. Above: complete spectrum; below: detail of the anodic contribution.
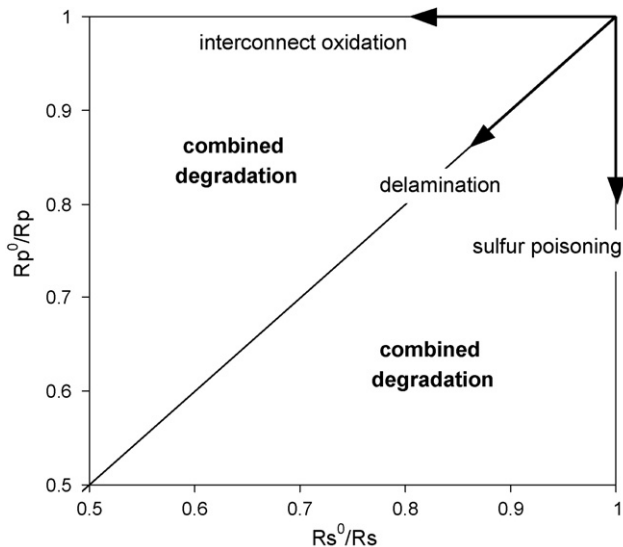
comparable extents of degradation occur. However, care must be taken with the use of this concept, since the resulting degradation path depends on characteristics of the intact cell, notably the supporting configuration. Fig. 11 shows the two degradation paths for our working example:

(a) Cathode delamination.
(b) Sulfur poisoning + oxide layer growth to produce an increase in R_s and R_p equivalent to (a), according to the degradation history shown in Table 4.

In this example, the large difference in degradation kinetics makes the two degradation paths different from each other. Sulfur adsorption kinetics are much faster than those of chromia growth, as illustrated in Fig. 11 (circles). The initial variation in polarization resistance in the case of delamination does not follow the 45° line because the portion of the cell under the first rib is only partially active in the intact case due to reactant starvation away from the channel. Therefore, inactivating it via cathode delamination does not cause as large an increase in polarization resistance as is observed when delaminating the portions of the cell away from the outside rib.

The combination of delamination with sulfur poisoning and, independently, with interconnect oxidation, are further illustrative examples of the application of the concepts explained in this section. In this case, the degradation scenario corresponds to the individual extents of degradation shown in Table 4, combined in two different ways, and for both electrolyte- and anode-supported configurations:

(a) delamination + interconnect oxidation;
(b) delamination + sulfur poisoning.

Fig. 10. Approximate overall degradation path followed by the mechanisms under study, when acting individually.
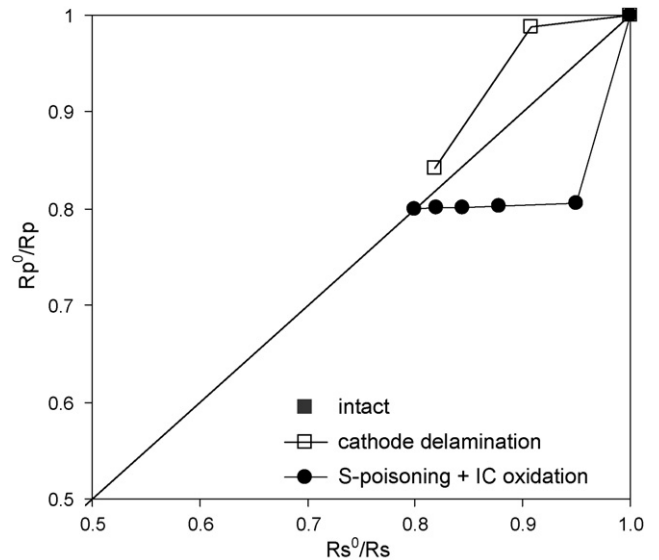

Fig. 11. Degradation path plot showing the normalized resistance behaviour of (●) inter-connect oxidation plus sulfur poisoning and (□) cathode delamination. Although the final degradation state is approximately the same for both cases, the difference in degradation history presents a possible way of distinguishing between the two cases.
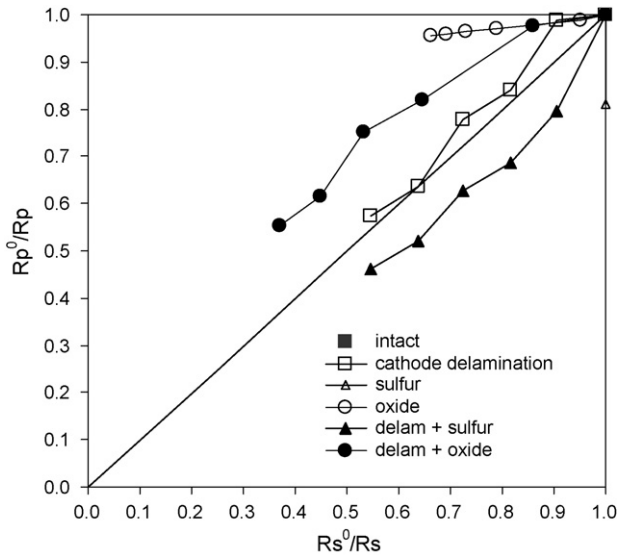
Fig. 12. Degradation path plots showing two different degradation scenarios: combination of delamination with interconnect oxidation (filled circles), and with sulfur poisoning (filled triangles). The delamination, oxide, and sulfur poisoning characteristic paths are shown for comparison. Electrolyte-supported configuration.

Fig. 12 shows these two combinations, compared with pure delamination, for the ESC configuration. The offset from the delamination characteristic line reflects the influence of interconnect oxidation and sulfur poisoning.

Fig. 13 shows the equivalent situation for the ASC configuration. The performance loss for the delamination + oxide layer case is in this case much more severe, because of the much higher relative importance of series resistance deterioration of the anode-supported cell.

The usefulness of the degradation path plot is subject to a-priori knowledge about the expected kinetics of the degradation modes, exemplified in this case by the much faster sulfur
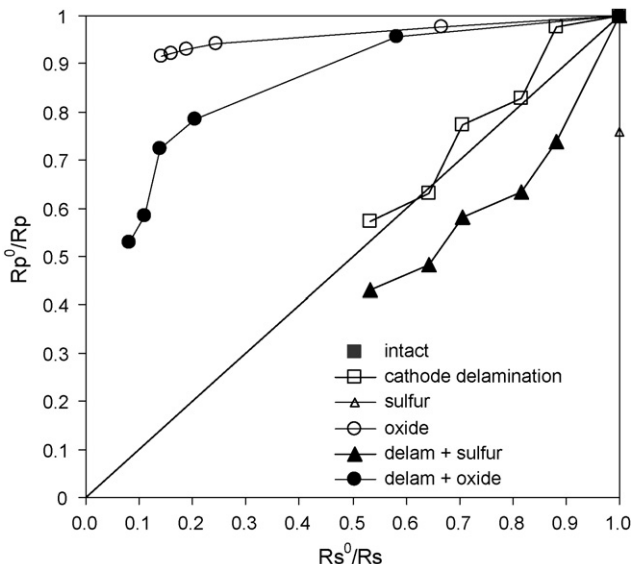
poisoning, compared with interconnect oxidation. In case of non-interacting multiple degradation modes simultaneously acting on a cell, it is possible to add their contributions to the degradation path plot. For N concurrent, non-interacting degradation mechanisms, the individual contributions to series and polarization resistance are additive:

$$R - R^0 = \Delta R = \sum_{k=1}^{N} \Delta R_k = \sum_{k=1}^{N} (R_k - R^0)$$

$$= \sum_{k=1}^{N} R_k - N R^0 \tag{3}$$

where R is either a polarization or a series resistance, ΔR indicates its change, and R^0 is the intact state series or polarization resistance. Now,

$$R - R^0 = \sum_{k=1}^{N} R_k - N R^0$$

$$\Rightarrow R = \sum_{k=1}^{N} R_k - (N-1) R^0$$

$$\Rightarrow \frac{R^0}{R} = \frac{R^0}{\sum_{k=1}^{N} R_k - (N-1) R^0} \tag{4}$$

$$\Rightarrow \frac{R^0}{R} = \frac{1}{\sum_{k=1}^{N} \frac{R_k}{R^0} - (N-1)}$$

Fig. 13. Degradation plot for the same combinations shown in Fig. 12, for the anode-supported configuration.
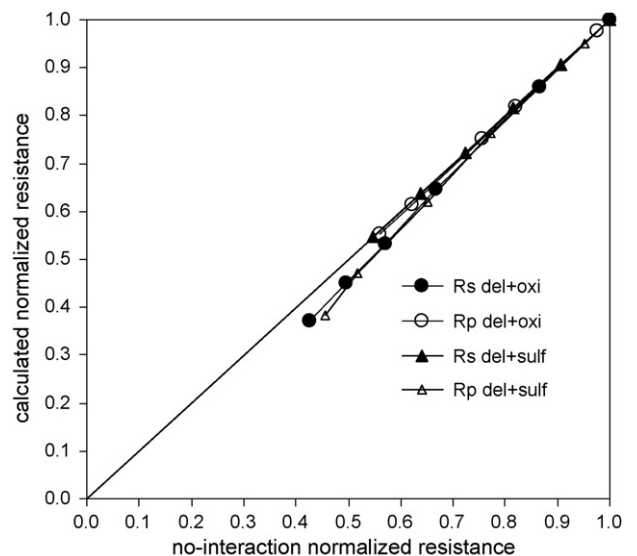

Fig. 14. Normalized resistance of the two combined degradation scenarios of the example above, as a function of the result of their direct addition, according to Eq. (5), with the assumption of no interaction. The plot indicates that the effects of the various degradation modes on the normalized polarization and series resistances are approximately independent of each other, and additive.

But R_k/R_0 is the reciprocal of the normalized resistance for the kth degradation mode, so

$$\frac{R^0}{R} = \frac{1}{\displaystyle\sum_{k=1}^{N}(1/(R^0/R_k)) - (N-1)} \tag{5}$$

This expression relates the normalized resistance for the multiple degradation state to the individual normalized resistances for each degradation mode. Plotting the result of Eq. (5) in a degradation path plot gives an idea of the relative influence of each degradation mode and their contribution to the overall degraded state. For known individual degradation mode behaviours, this equation gives the result of their combination, under the assumption of no interaction. As an application example, Fig. 14 shows the normalized resistances for the combined degradation modes shown above, calculated using the model, as a function of the combined normalized resistances calculated using Eq. (5), i.e. adding the individual effects assuming no interaction. The small deviation from the $x = y$ line indicates only weak interaction between each pair of degradation modes.

3. Conclusions

As the second part of our SOFC degradation diagnosis modeling series, the purpose of this paper is twofold:

1. To evaluate the robustness of the normalized resistance results obtained in Part I to input parameter variability.
2. To assess the model predictive capability in the presence of two simultaneous degradation modes.

A parametric study consisting of solving for the polarization and series resistances for a wide but reasonable range of input parameters revealed some of the strengths and limitations of the method. Repeated for all degradation modes under study, this parameterization revealed that the results for delamination are very robust to inaccuracies in the knowledge of, or interactions among, cell parameters.

An equivalent conclusion applies to oxide layer growth and interconnect detachment, but to a lesser extent. In the case of oxide layer growth, the parameters that most influence repeatability are the main charge transfer coefficients, the exchange current densities, and the operating point. Interconnect detachment variability on the cathode-side mostly depends on the parameters that determine the cathode electronic conductance. Detachment at the anode/interconnect interface is much less affected by parameter variability due to the very high electronic conductivity of nickel, especially for thick anode support configurations.

In contrast, the results for sulfur poisoning are strongly dependent on the operating conditions and cell characteristics, especially the operating point and the charge transfer coefficients.

Simulating two concurrent degradation modes challenged the diagnosis capability of the proposed method. Modeling results indicate that the convolution of the impedance spectrum features may hinder individual diagnosis of each mode. Tracking the electrode characteristic arc (or peak), and/or the degradation path, provides further insight to the diagnostic technique, but some a-priori knowledge of the expected kinetics of the different mechanisms is essential. The degradation path plot constitutes a useful tool for the visualization of the degradation history of the cell.

References

[1] J.I. Gazzarri, O. Kesler, J. Power Sources 176 (2008) 138–154.
[2] J.I. Gazzarri, O. Kesler, J. Power Sources 167 (2) (2007) 430–441.
[3] J.I. Gazzarri, O. Kesler, J. Power Sources 167 (1) (2007) 100–110.
[4] http://www.math.hkbu.edu.hk/UniformDesign/.
[5] S. Xia, V. Birss, Proceedings of the SOFC IX, vol. 2, 2005, pp. 1275–1283.
[6] S. Zha, Z. Cheng, M. Liu, J. Electrochem. Soc. 154 (2) (2007) B201–B206.
[7] Y. Matsuzaki, I. Yasuda, Solid State Ionics 132 (2000) 261–269.
[8] J. Piña, V. Bucalá, D. Borio, Int. J. Chem. React. Eng. A 11 (2003) 1–20.
[9] J.-H. Park, K. Natesan, Oxid. Met. 33 (1–2) (1990) 31–53.
[10] T. Brylewski, et al., Solid State Ionics 143 (2001) 131–150.
[11] J. Gazzarri, PhD Thesis, University of British Columbia, Canada (2007).
[12] H. Schichlein, A. Müller, M. Voigts, A. Krügel, E. Ivers-Tiffée, J. Appl. Electrochem. 32 (8) (2002) 875–882.